

Kaniadakis holographic dark energy: observational constraints and global dynamics

A. Hernández-Almada¹, Genly Leon² Juan Magaña³ Miguel A. García-Aspeitia^{4,5}, V. Motta⁶, Emmanuel N. Saridakis^{7,8,9}, Kuralay Yesmakhanova^{9,10}

¹Facultad de Ingeniería, Universidad Autónoma de Querétaro, Centro Universitario Cerro de las Campanas, 76010, Santiago de Querétaro, México

²Departamento de Matemáticas, Universidad Católica del Norte, Avda. Angamos 0610, Casilla 1280 Antofagasta, Chile

³Instituto de Astrofísica & Centro de Astro-Ingeniería, Pontificia Universidad Católica de Chile, Av. Vicuña Mackenna, 4860, Santiago, Chile

⁴Universidad Autónoma de Zacatecas, Calzada Solidaridad esquina con Paseo a la Bufa S/N C.P. 98060, Zacatecas, México

⁵Consejo Nacional de Ciencia y Tecnología,
Av. Insurgentes Sur 1582. Colonia Crédito Constructor, Del. Benito Juárez C.P. 03940, Ciudad de México, México

⁶Instituto de Física y Astronomía, Facultad de Ciencias, Universidad de Valparaíso, Avda. Gran Bretaña 1111, Valparaíso, Chile

⁷National Observatory of Athens, Lofos Nymfon, 11852 Athens, Greece

⁸CAS Key Laboratory for Researches in Galaxies and Cosmology, Department of Astronomy, University of Science and Technology of China, Hefei, Anhui 230026, P.R. China

⁹Ratbay Myrzakulov Eurasian International Centre for Theoretical Physics, Nur-Sultan 010009, Kazakhstan

¹⁰Eurasian National University, Nur-Sultan Astana 010008, Kazakhstan.

E-mail: ahalmada@uaq.mx, genly.leon@ucn.cl, aldebaran.99@gmail.com,
aspeitia@fisica.uaz.edu.mx, veronica.motta@uv.cl, msaridak@noa.gr,
kryesmakhanova@gmail.com

Abstract. We investigate Kaniadakis-holographic dark energy by confronting it with observations. We perform a Markov Chain Monte Carlo analysis using cosmic chronometers, supernovae type Ia, and Baryon Acoustic Oscillations data. Concerning the Kaniadakis parameter, we find that it is constrained around zero, namely around the value in which Kaniadakis entropy recovers standard Bekenstein-Hawking one. Additionally, for the present matter density parameter $\Omega_m^{(0)}$, we obtain a value slightly smaller compared to Λ CDM scenario. However, for the present dimensionless Hubble constant, the combined dataset analysis gives $h = 0.722_{-0.010}^{+0.010}$, which is consistent within 1σ with its direct measurements through Cepheids, thus Kaniadakis-holographic dark energy offers an alleviation to the H_0 tension. Furthermore, we reconstruct the evolution of the Hubble, deceleration and jerk parameters extracting the deceleration-acceleration transition redshift as $z_T = 0.65_{-0.11}^{+0.13}$. Finally, performing a detailed local and global dynamical system analysis, we find that the past attractor of the Universe is the matter-dominated solution, while the late-time stable solution is the dark-energy-dominated one.

Keywords: Holographic Dark Energy, Observational Constraints, Dynamical System Analysis, Kaniadakis entropy

Contents

1	Introduction	1
2	Kaniadakis holographic dark energy	2
3	Observational analysis	7
3.1	Data and methodology	7
3.1.1	Cosmic chronometer data	7
3.1.2	Pantheon SNIa sample	7
3.1.3	Baryon Acoustic Oscillations	8
3.1.4	Bayesian analysis	8
3.2	Results from observational constraints	9
4	Dynamical system and stability analysis	12
4.1	Local dynamical system formulation	12
4.2	Global dynamical systems formulation	14
4.2.1	Standard holographic dark energy ($\beta = 0$)	15
4.2.2	Kaniadakis holographic dark energy ($\beta \neq 0$)	17
5	Summary and discussion	20

1 Introduction

The acceleration of the Universe is one of the most elusive problems in modern cosmology. Since its discovery in the last decade of the twentieth century by Supernovae (SNIa) observations [1, 2], and its confirmation by the acoustic peaks of the cosmic microwave background (CMB) radiation [3], it has been a theoretical and observational challenge to construct a model that combines all of its characteristics. From a theoretical point of view, and assuming homogeneous and isotropic symmetries (cosmological principle), the need for a component with features able to reproduce the Universe acceleration is vital to obtain accurate values for the observable Universe age and size. Recently, the confidence in the detection of this acceleration at late times has been increased with precise observations of the large scale structure [4].

The best candidate to explain the observed acceleration is the well-known Cosmological Constant (CC), interpreted under the assumption that quantum vacuum fluctuations generate the constant energy density observed and, with this, a late-time acceleration. However, when we apply the Quantum Field Theory to assess the energy density, the result is in total discrepancy with observations, giving rise to the so-called *fine-tuning problem* [5, 6]. In addition, recent observations developed by the collaboration *Supernova H₀ for the Equation of State* (SH0ES) [7] show a discrepancy for the obtained value of H_0 when compared to Planck observations based on the Λ Cold Dark Matter (Λ CDM) model [8]. This generates a tension of 4.2σ between the mentioned experiments, bringing a new crisis and the need for new ways to tackle the problem [9], as long as this discrepancy is not related to unknown systematic errors affecting the measurements [10–14]. Is in this vein that the community has been proposing other alternatives to address the problem of the Universe acceleration. In

general, there are two main directions that one could follow. The first is to maintain general relativity and introduce new peculiar forms of matter, such as scalar fields [15–17], Chaplygin gas [18–20], viscous fluids [21–26], etc, collectively known as dark-energy sector. The second way is to construct modified gravitational theories [27, 28] such as braneworlds models [29–31], emergent gravity [32–37], Einstein-Gauss-Bonet [38, 39], thermodynamical models [40, 41], torsional gravity [42], etc.

On the other hand, there is an increasing interest in dark energy alternative models with the holographic principle. This is inspired by the relation between entropy and the area of a black hole. It states that the observable degree of freedom of a physical system in a volume can be encoded in a lower-dimensional description on its boundary [43, 44]. The holographic principle imposes a connection between the infrared (IR) cutoff, related to large-scale of the Universe, with the ultraviolet (UV) one, related to the vacuum energy. Application of the holographic principle to the Universe horizon gives rise to a vacuum energy of holographic origin, namely holographic dark energy [45, 46]. Holographic dark energy proves to lead to interesting phenomenology and, thus, it has been studied in detailed [45–53], confronted to observations [54–59] and extended to various frameworks [60–81].

Recently, an extension of the holographic dark energy scenario was constructed in [82], based on Kaniadakis entropy. The latter is an extended entropy arising from the relativistic extension of standard statistical theory, quantified by one new parameter [83, 84]. In the case where this Kaniadakis parameter becomes zero, i.e. when Kaniadakis entropy becomes the standard Bekenstein-Hawking entropy, Kaniadakis-holographic dark energy recovers standard-holographic dark energy, however, in the general case, it exhibits a range of behaviors with interesting cosmological implications.

In this work, we investigate Kaniadakis-holographic dark energy, in order to tackle the late time universe acceleration problem. The outline of the paper is as follows. In Section 2 the mathematical background of the model is considered, presenting the master equations. Section 3 presents the observational confrontation analysis that includes three data samples and the results from the corresponding constraints. Section 4 is dedicated to the dynamical system investigation and the stability analysis. Finally, in Section 5 we give a brief summary and a discussion of the results. Throughout the manuscript we use natural units where $\tilde{c} = \hbar = k_B = 1$ (unless stated otherwise).

2 Kaniadakis holographic dark energy

In this section we briefly review Kaniadakis holographic dark energy and we elaborate the corresponding equations in order to bring them to a form suitable for observational confrontation. The essence of holographic dark energy is the inequality $\rho_{DE}L^4 \leq S$, with ρ_{DE} being the holographic dark energy density, L the largest distance (typically a horizon), and S the entropy expression in the case of a black hole with a horizon L [45, 46]. In the standard application using Bekenstein-Hawking entropy $S_{BH} \propto A/(4G) = \pi L^2/G$, where A is the area and G the Newton's constant, one obtains standard-holographic dark energy, i.e. $\rho_{DE} = 3c^2 M_p^2 L^{-2}$, where $M_p^2 = (8\pi G)^{-1}$ is the Planck mass and c is the model parameter arising from the saturation of the above inequality.

On the other hand, one can construct the one-parameter generalization of the classical entropy, namely Kaniadakis entropy $S_K = -k_B \sum_i n_i \ln_{\{K\}} n_i$ [83, 84], where k_B is the Boltzmann constant and with $\ln_{\{K\}} x = (x^K - x^{-K})/2K$. This is characterized by the dimensionless parameter $-1 < K < 1$, which accounts for the relativistic deviations from standard statisti-

cal mechanics, and in the limit $K \rightarrow 0$ it recovers standard entropy. Kaniadakis entropy can be re-expressed as [85–87]

$$S_K = -k_B \sum_{i=1}^W \frac{P_i^{1+K} - P_i^{1-K}}{2K}, \quad (2.1)$$

where P_i is the probability of a specific microstate of the system and W the total number of possible configurations. Applied in the black-hole framework, it results into [82, 88, 89]

$$S_K = \frac{1}{K} \sinh(KS_{BH}), \quad (2.2)$$

which gives standard Bekenstein-Hawking entropy in the limit $K \rightarrow 0$. Finally, since any deviations from standard thermodynamics are expected to be small, one can approximate (2.2) for $K \ll 1$, acquiring [82]

$$S_K = S_{BH} + \frac{K^2}{6} S_{BH}^3 + \mathcal{O}(K^4). \quad (2.3)$$

In order to analyze the dynamics of the universe, we consider the homogeneous and isotropic cosmology based on the Friedmann-Lemaître-Robertson-Walker (FLRW) line element $ds^2 = -dt^2 + a(t)(dr^2 + r^2 d\Omega^2)$, where $d\Omega^2 \equiv d\theta^2 + \sin^2 \theta d\varphi^2$, $a(t)$ is the scale factor and we consider null spatial curvature $k = 0$. Furthermore, as usual we use L as the future event horizon $R_h \equiv a \int_t^\infty \frac{1}{a(s)} ds$. Inserting these into the above formulation, and using Kaniadakis entropy instead of Bekenstein-Hawking one, we extract the energy density of Kaniadakis holographic dark energy as [82]

$$\rho_{DE} = \frac{3c^2 M_p^2}{R_h^2} + K^2 M_p^6 R_h^2, \quad (2.4)$$

with $c > 0$ and K being the two parameters of the model. Hence, we can write the Friedmann and Raychaudhuri equations as

$$H^2 = \frac{1}{3M_p^2}(\rho_m + \rho_{DE}), \quad (2.5)$$

$$\dot{H} = -\frac{1}{2M_p^2}(\rho_m + p_m + \rho_{DE} + p_{DE}), \quad (2.6)$$

where $H \equiv \dot{a}/a$ is the Hubble parameter, ρ_m and p_m are the energy density and pressure of matter perfect fluid, while the matter conservation leads to dark energy conservation and, in turn, to the dark energy pressure

$$p_{DE} = -\frac{2c^2 M_p^2}{R_h^3 H} - \frac{c^2 M_p^2}{R_h^2} + K^2 M_p^6 \left[\frac{2R_h}{3H} - \frac{5}{3} R_h^2 \right]. \quad (2.7)$$

The combination of Raychaudhuri equation (2.6) and (2.4), (2.7) gives

$$\dot{H} = \frac{c^2}{R_h^3 H} + \frac{c^2(3w_m + 1)}{2R_h^2} - \frac{3}{2}(w_m + 1)H^2 - K^2 M_p^4 \left[\frac{R_h}{3H} - \frac{1}{6} R_h^2 (3w_m + 5) \right], \quad (2.8)$$

where $w_m \equiv p_m/\rho_m$ is the equation of state (EoS) parameter for matter, considered from now on as dust ($w_m = 0$). From this expression we can construct the deceleration and jerk

parameters, which give us information about the transition to an accelerated Universe. Thus, using the definition of R_h , we obtain that the energy density is

$$\rho_{DE} = \frac{3c^2 M_p^2}{a^2 \left(\int_t^\infty \frac{1}{a(s)} ds \right)^2} + K^2 M_p^6 a^2 \left(\int_t^\infty \frac{1}{a(s)} ds \right)^2, \quad (2.9)$$

and the pressure

$$\begin{aligned} p_{DE} = & - \frac{2c^2 M_p^2}{a^3 H \left(\int_t^\infty \frac{1}{a(s)} ds \right)^3} - \frac{c^2 M_p^2}{a^2 \left(\int_t^\infty \frac{1}{a(s)} ds \right)^2} \\ & + K^2 M_p^6 \left[\frac{2a \left(\int_t^\infty \frac{1}{a(s)} ds \right)}{3H} - \frac{5}{3} a^2 \left(\int_t^\infty \frac{1}{a(s)} ds \right)^2 \right]. \end{aligned} \quad (2.10)$$

Moreover, the fractional energy density of DE is defined as

$$\Omega_{DE} := \frac{\rho_{DE}}{3M_p^2 H^2} = \frac{K^2 M_p^6 a^4 \left(\int_t^\infty \frac{1}{a(s)} ds \right)^4 + 3c^2 M_p^2}{3M_p^2 a^2 H^2 \left(\int_t^\infty \frac{1}{a(s)} ds \right)^2}. \quad (2.11)$$

From definition (2.11) we have four branches for

$$\mathcal{I}(t) := \int_t^\infty \frac{1}{a(s)} ds, \quad (2.12)$$

which give four possible expressions for the particle horizon

$$R_{h1,2}(t) = \mp \frac{\left[3H^2 \Omega_{DE} - \sqrt{9H^4 \Omega_{DE}^2 - 12c^2 K^2 M_p^4} \right]^{1/2}}{\sqrt{2} K M_p^2}, \quad (2.13)$$

$$R_{h3,4}(t) = \mp \frac{\left[3H^2 \Omega_{DE} + \sqrt{9H^4 \Omega_{DE}^2 - 12c^2 K^2 M_p^4} \right]^{1/2}}{\sqrt{2} K M_p^2}. \quad (2.14)$$

$R_{h1}(t)$ and $R_{h3}(t)$ are both discarded since they lead to negative particle horizon. To decide between the choices $R_{h2}(t)$ and $R_{h4}(t)$, which are both non negative, we calculate the limit $K \rightarrow 0$ and obtain

$$\lim_{K \rightarrow 0} R_{h2} = \frac{c}{H \sqrt{\Omega_{DE}}}, \quad \lim_{K \rightarrow 0} R_{h4} = \infty. \quad (2.15)$$

That is, $R_{h2}(t)$ defined by (2.13) is the only physical solution.

We proceed by introducing the usual dimensionless variable

$$E \equiv \frac{H}{H_0}, \quad (2.16)$$

where H_0 is the Hubble constant at present time and, for convenience, we define the dimensionless constant

$$\beta \equiv \frac{K M_p^2}{H_0^2}, \quad (2.17)$$

Differentiating (2.11) and (2.16), and using the Friedmann equations we obtain the master equations

$$\Omega'_{DE} = (1 - \Omega_{DE}) [3(w_m + 1)\Omega_{DE} + 2\mathcal{X}], \quad (2.18)$$

$$E' = E \left[-\frac{3}{2}(w_m + 1)(1 - \Omega_{DE}) + \mathcal{X} \right], \quad (2.19)$$

where

$$\mathcal{X} \equiv \frac{1}{E^3} \left[\frac{2\beta^2 E^4 \Omega_{DE}^2 - 8\beta^4 c^2/3}{3E^2 \Omega_{DE} - \sqrt{9E^4 \Omega_{DE}^2 - 12\beta^2 c^2}} \right]^{1/2} - \frac{1}{E^2} [E^4 \Omega_{DE}^2 - 4\beta^2 c^2/3]^{1/2}. \quad (2.20)$$

We use initial conditions $\Omega_{DE}(0) \equiv \Omega_{DE}^{(0)} = 1 - \Omega_m^{(0)}$, $E(0) = 1$, where primes denote derivatives with respect to e-foldings number $N = \ln(a/a_0)$, and $N = 0$ marks the current time (from now on, the index “0” marks the value of a quantity at present). The physical region of the phase space is

$$3E^4 \Omega_{DE}^2 - 4\beta^2 c^2 \geq 0. \quad (2.21)$$

Notice that $\mathcal{X} \rightarrow \frac{\Omega_{DE}^{3/2}}{c} - \Omega_{DE}$ as $\beta \rightarrow 0$.

From the matter conservation equation, we arrive at

$$\rho'_m(N) = -3(1 + w_m)\rho_m, \quad \rho_m(0) = 3M_p^2 H_0^2 \Omega_m^{(0)}, \quad (2.22)$$

and, therefore, we have $\rho_m(N) = 3H_0^2 M_p^2 \Omega_m^{(0)} e^{-3N(w_m+1)}$ which then leads to

$$\Omega_{DE}(N) = 1 - \Omega_m(N) = 1 - \frac{\Omega_m^{(0)} e^{-3N(w_m+1)}}{E^2}. \quad (2.23)$$

Defining $Z = E^2$, we obtain the equation

$$Z' = -3(w_m + 1)\Omega_m^{(0)} e^{-3N(w_m+1)} + 2\mathcal{X}Z, \quad Z(0) = 1, \quad (2.24)$$

where

$$\begin{aligned} \mathcal{X}Z = & - \left[\left(\Omega_m^{(0)} e^{-3N(w_m+1)} - Z \right)^2 - \frac{4\beta^2 c^2}{3} \right]^{1/2} \\ & + \left[\frac{2\beta^2 \left(Z - \Omega_m^{(0)} e^{-3N(w_m+1)} \right)^2 - \frac{8\beta^4 c^2}{3}}{3Z^2 - 3Z\Omega_m^{(0)} e^{-3N(w_m+1)} - Z\sqrt{9 \left(Z - \Omega_m^{(0)} e^{-3N(w_m+1)} \right)^2 - 12\beta^2 c^2}} \right]^{1/2}. \end{aligned} \quad (2.25)$$

Thus, the evolution of $E^2(z)$ can be obtained by substituting (2.25) into (2.24). More precisely, substituting (2.25) into (2.24), integrating, and imposing the initial condition $Z(0) = 1$, gives $E^2(N)$. In order to express it as $E^2(z)$, we use the relation $N = \ln(a/a_0) = -\ln(1+z)$, which is a relation between the e-folding (N), the scale factor (a), and the redshift (z).

Additionally, we can now write the deceleration parameter $q(z)$, and a cosmographic parameter which is related to the third-order derivative of the scale factor, i.e. the cosmographic jerk parameter $j(z)$, which are given by the formulas

$$q := -1 - \frac{E'}{E}, \quad (2.26)$$

$$j := q(2q + 1) - q', \quad (2.27)$$

where $j = 1$ corresponds to the case of a cosmological constant.

Hence, equation (2.26) becomes

$$q = -1 + \frac{3}{2}(w_m + 1)(1 - \Omega_{DE}) + \frac{\sqrt{E^4\Omega_{DE}^2 - \frac{4\beta^2c^2}{3}}}{E^2} - \frac{\beta\sqrt{2E^4\Omega_{DE}^2 - \frac{8\beta^2c^2}{3}}}{E^3\sqrt{3E^2\Omega_{DE} - \sqrt{9E^4\Omega_{DE}^2 - 12\beta^2c^2}}}.$$
(2.28)

j is found by direct evaluation of (2.27). We have mentioned before that taking the limit $\beta \rightarrow 0$ in (2.18) and (2.19), and neglecting error terms $O(\beta^2)$, we acquire the approximated differential equations

$$\Omega'_{DE} = \frac{\Omega_{DE}(1 - \Omega_{DE})(3w_m c + c + 2\sqrt{\Omega_{DE}})}{c},$$
(2.29a)

and

$$E' = \frac{E \left\{ 2\Omega_{DE}^{3/2} + c[3w_m(\Omega_{DE} - 1) + \Omega_{DE} - 3] \right\}}{2c}.$$
(2.29b)

Imposing the conditions

$$E(\Omega_{DE}^{(0)}) = 1, \quad \ln \left(\frac{a}{a_0} \right) \Big|_{\Omega_{DE}^{(0)}} = 0,$$
(2.29c)

we obtain the implicit solutions

$$E = \left(\frac{\Omega_{DE}}{\Omega_{DE}^{(0)}} \right)^{-\frac{3(w_m+1)}{6w_m+2}} \left(\frac{1 - \sqrt{\Omega_{DE}}}{1 - \sqrt{\Omega_{DE}^{(0)}}} \right)^{\frac{c-1}{3cw_m+c+2}} \left(\frac{\sqrt{\Omega_{DE}} + 1}{\sqrt{\Omega_{DE}^{(0)}} + 1} \right)^{\frac{c+1}{3cw_m+c-2}} \times \left(\frac{3cw_m + c + 2\sqrt{\Omega_{DE}}}{3cw_m + c + 2\sqrt{\Omega_{DE}^{(0)}}} \right)^{-\frac{12(w_m+1)}{(3w_m+1)((3cw_m+c)^2-4)}},$$
(2.29d)

and

$$(1+z)^{-1} := \left(\frac{a}{a_0} \right) = \left(\frac{\Omega_{DE}}{\Omega_{DE}^{(0)}} \right)^{\frac{1}{3w_m+1}} \left(\frac{1 - \sqrt{\Omega_{DE}}}{1 - \sqrt{\Omega_{DE}^{(0)}}} \right)^{-\frac{c}{3cw_m+c+2}} \left(\frac{\sqrt{\Omega_{DE}} + 1}{\sqrt{\Omega_{DE}^{(0)}} + 1} \right)^{-\frac{c}{3cw_m+c-2}} \times \left(\frac{3cw_m + c + 2\sqrt{\Omega_{DE}}}{3cw_m + c + 2\sqrt{\Omega_{DE}^{(0)}}} \right)^{\frac{8}{(3w_m+1)((3cw_m+c)^2-4)}}.$$
(2.29e)

Lastly, expanding around $\beta = 0$ and $\Omega_{DE} = 1$ and removing second order terms, the deceleration parameter (2.26) and the cosmographic jerk parameter (2.27) (in the dark-energy dominated epoch) are given by

$$q = -\frac{1}{c} + \frac{(1 - \Omega_{DE})(3cw_m + c + 3)}{2c},$$
(2.29f)

$$j = \frac{2 - c}{c^2} + \frac{(1 - \Omega_{DE})(3cw_m + c + 3)[c(3w_m + 2) - 2]}{2c^2}.$$
(2.29g)

Furthermore, expanding around $\beta = 0$ and $\Omega_{DE} = 0$ and removing second order terms, the deceleration parameter (2.26) and the cosmographic jerk parameter (2.27) (in the matter dominated epoch) are given by

$$q = \frac{1}{2}(3w_m + 1)(1 - \Omega_{DE}), \quad (2.29h)$$

$$j = \frac{1}{2}[9w_m(w_m + 1) + 2](1 - \Omega_{DE}). \quad (2.29i)$$

Equations (2.29) characterize standard holographic cosmology.

3 Observational analysis

One of the goals of this work is to provide observational bounds on the parameter of Kaniadakis entropy K or, more conveniently β , however we are also interested in the behavior of all cosmological parameters, namely on the vector $\Theta = \{h, \Omega_m^{(0)}, \beta, c\}$. For the parameter estimation we use the recent measurements of the observational Hubble data as well as data from type Ia supernovae, and baryon acoustic oscillations observations. In what follows, we first briefly introduce these datasets and the Bayesian methodology, and then we apply it in the scenario of Kaniadakis-holographic dark energy, providing the resulting observational constraints.

3.1 Data and methodology

3.1.1 Cosmic chronometer data

The Hubble parameter $H(z)$ describes the expansion rate of the Universe as a function of redshift z . Currently, this parameter can be estimated from baryon acoustic oscillations measurements and differential age in passive galaxies (dubbed as cosmic chronometers). While the former could be biased due to the assumption of a fiducial cosmology, the samples from cosmic chronometers are independent from the underlying cosmological model. Thus, in this work we only consider the 31 points from cosmic chronometer sample presented in [90, 91] in the redshift range $0.07 < z < 1.965$. We assume a Gaussian likelihood function for this observation as $\mathcal{L}_{CC} \propto \exp(-\chi_{CC}^2/2)$, where the figure-of-merit is

$$\chi_{CC}^2 = \sum_i^{31} \left[\frac{H_{mod}(\Theta, z_i) - H_{dat}(z_i)}{\sigma_{dat}^i} \right]^2, \quad (3.1)$$

where $H_{dat}(z_i)$ and σ_{obs}^i are the measured Hubble parameter and its observational uncertainty at the redshift z_i , respectively. The predicted Hubble parameter by the Kaniadakis-holographic dark energy is denoted by $H_{mod}(\Theta)$, and it can be obtained by solving the system of equations (2.18)-(2.20).

3.1.2 Pantheon SNIa sample

Since the discovery of the late cosmic acceleration with the observations of high redshift type Ia supernovae (SNIa) by [1, 2], the observation of these distant objects is a crucial test to determine if a cosmological scenario is a viable candidate for the description of the late-time Universe. The probe consists of confronting the observed luminosity distance (or distance module) of SNIa with the theoretical prediction of any model. Up to now, the Pantheon

sample [92] is the largest collection of high-redshift SNIa, with 1048 data points with measured redshifts in the range $0.001 < z < 2.3$. The authors also provide a binned sample containing 40 points of binned distances $\mu_{dat,bin}$ in the redshift range $0.014 < z < 1.61$. In this work, we use the binned set and we consider a Gaussian likelihood $\mathcal{L}_{SNIa} \propto \exp(-\chi_{SNIa}^2/2)$. By marginalizing the nuisance parameters, the figure-of-merit function χ_{SNIa}^2 is given by

$$\chi_{SNIa}^2 = a + \log\left(\frac{e}{2\pi}\right) - \frac{b^2}{e}, \quad (3.2)$$

where $a = \Delta\tilde{\mu}^T \cdot \mathbf{C}_P^{-1} \cdot \Delta\tilde{\mu}$, $b = \Delta\tilde{\mu}^T \cdot \mathbf{C}_P^{-1} \cdot \Delta\mathbf{1}$, $e = \Delta\mathbf{1}^T \cdot \mathbf{C}_P^{-1} \cdot \Delta\mathbf{1}$, and $\Delta\tilde{\mu}$ is the vector of residuals between the model distance modulus and the observed (binned) one. The covariance matrix \mathbf{C}_P takes into account systematic and statistical uncertainties [92]. Moreover, the theoretical counterpart of the distance modulus for any cosmological model is given by $\mu_{mod}(\Theta, z) = 5 \log_{10} (d_L(\Theta, z)/10\text{pc})$, where d_L is the luminosity distance given by

$$d_L(\Theta, z) = \frac{\tilde{c}}{H_0} (1+z) \int_0^z \frac{dz'}{E(z')}, \quad (3.3)$$

where \tilde{c} is the light speed.

3.1.3 Baryon Acoustic Oscillations

Baryon Acoustic Oscillations (BAO) are fluctuation patterns in the matter density field as result of internal interactions in the hot primordial plasma during the pre-recombination stage. Based on luminous red galaxies, a sample of 15 transversal BAO scale measurements within the redshift $0.110 < z < 2.225$ were collected by [93]. Assuming a Gaussian likelihood, $\mathcal{L}_{BAO} \propto \exp(-\chi_{BAO}^2/2)$, we build the figure of merit function as

$$\chi_{BAO}^2 = \sum_{i=1}^{15} \left[\frac{\theta_{dat}^i - \theta_{mod}(\Theta, z_i)}{\sigma_{\theta_{dat}^i}} \right]^2, \quad (3.4)$$

where $\theta_{dat}^i \pm \sigma_{\theta_{dat}^i}$ is the BAO angular scale and its uncertainty at 68% measured at z_i . The theoretical BAO angular scale counterpart, denoted as θ_{mod} , is estimated by

$$\theta_{mod}(z) = \frac{r_{drag}}{(1+z)D_A(z)}, \quad (3.5)$$

where $D_A = d_L(z)/(1+z)^2$ is the angular diameter distance at z which depends on the dimensionless luminosity distance $d_L(z)$, and r_{drag} is the sound horizon at the baryon drag epoch, considered to be $r_{drag} = 147.21 \pm 0.23$ [94].

3.1.4 Bayesian analysis

A Bayesian statistical analysis based on Markov Chain Monte Carlo (MCMC) algorithm is performed to bound the free parameters of the Kaniadakis-holographic dark energy. The MCMC approach is implemented through the `emcee` python module [95] in which we generate 1000 chains with 250 steps, each one after a burn-in phase. The latter is stopped when the chains have converged based on the auto-correlation time criteria. Thus, the inference of the parameter space is obtained by minimizing a Gaussian log-likelihood, $-2 \ln(\mathcal{L}_{data}) \propto \chi_{data}^2$, considering flat priors in the intervals: $h \in [0.2, 1]$, $\Omega_m^{(0)} \in [0, 1]$, $\beta \in [-1, 1]$, $c \in [0, 2]$ for each

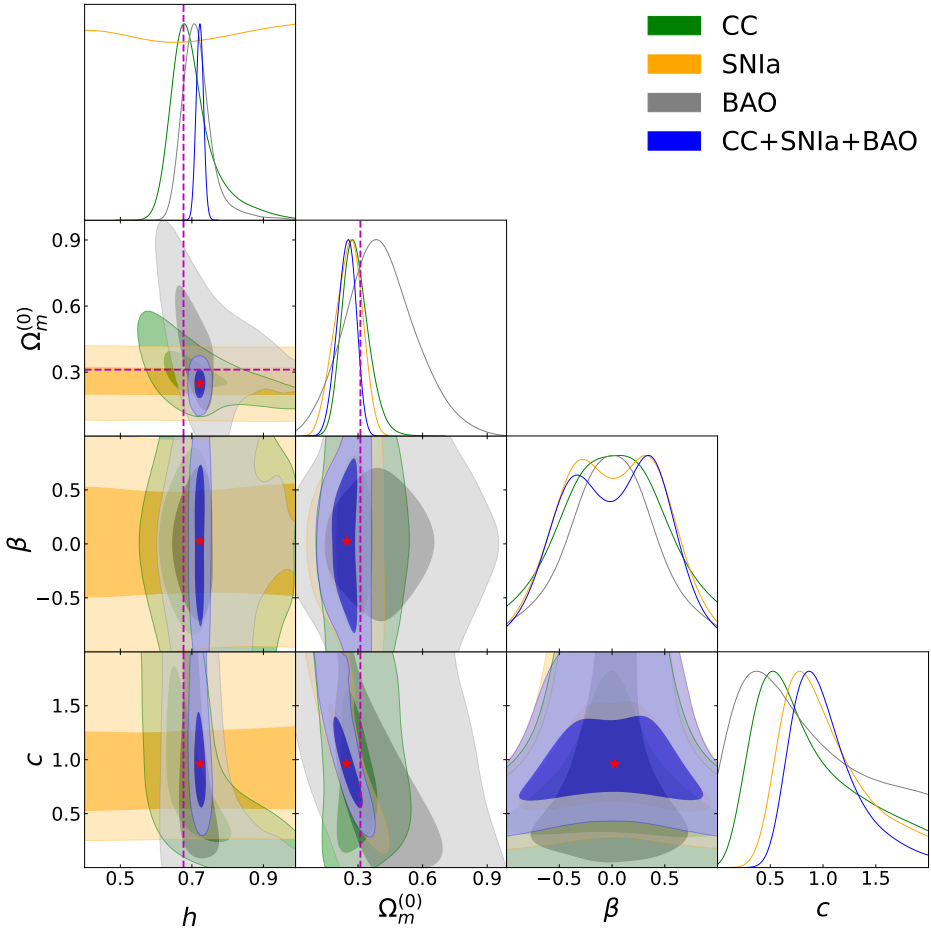


Figure 1. Two-dimensional likelihood contours at 68% and 99.7% confidence level (CL), alongside the corresponding 1D posterior distribution of the free parameters, in Kaniadakis-holographic dark energy case. The stars denote the mean values using the joint analysis, and the dashed lines represent the best-fit values for Λ CDM cosmology [8].

dataset. Additionally, a combined analysis is performed by assuming no correlation between the datasets, hence the figure of merit is

$$\chi_{\text{Joint}}^2 = \chi_{\text{CC}}^2 + \chi_{\text{SNIa}}^2 + \chi_{\text{BAO}}^2, \quad (3.6)$$

namely, the sum of the χ^2 corresponding to each sample as previously defined.

3.2 Results from observational constraints

We perform the full confrontation described above for the scenario of Kaniadakis holographic dark energy, and in Fig. 1 we present the 2D parameter likelihood contours at 68% (1 σ) and 99.7% (3 σ) confidence level (CL) respectively, alongside the corresponding 1D posterior distribution of the parameters. Additionally, Table 1 shows the mean values of the parameters and their uncertainties at 1 σ .

In order to statistically compare these results with Λ CDM cosmology, we apply the corrected Akaike information criterion (AICc) [96–98] and the Bayesian information criterion (BIC) [99]. They give a penalty according to size of data sample (N) and the number

Sample	χ^2	h	$\Omega_m^{(0)}$	β	c	ΔAICc	ΔBIC
CC	14.69	$0.690^{+0.072}_{-0.043}$	$0.284^{+0.066}_{-0.055}$	$0.012^{+0.486}_{-0.489}$	$0.729^{+0.665}_{-0.350}$	5.2	7.0
SNIa	48.52	$0.597^{+0.279}_{-0.271}$	$0.259^{+0.059}_{-0.069}$	$0.013^{+0.480}_{-0.482}$	$0.932^{+0.492}_{-0.302}$	5.1	7.5
BAO	12.98	$0.711^{+0.041}_{-0.035}$	$0.400^{+0.171}_{-0.148}$	$-0.001^{+0.415}_{-0.417}$	$0.736^{+0.762}_{-0.469}$	8.1	5.5
CC+SNIa+BAO	80.94	$0.722^{+0.010}_{-0.010}$	$0.248^{+0.041}_{-0.046}$	$0.026^{+0.456}_{-0.507}$	$0.962^{+0.375}_{-0.245}$	4.1	9.0

Table 1. Mean values of various parameters and their 68% CL uncertainties for Kaniadakis-holographic dark energy. The quantities ΔAICc (ΔBIC) are the differences with respect to ΛCDM paradigm.

of degrees of freedom (k) defined as $\text{AICc} = \chi_{min}^2 + 2k + (2k^2 + 2k)/(N - k - 1)$ and $\text{BIC} = \chi_{min}^2 + k \log(N)$ respectively, where χ_{min}^2 is the minimum value of the χ^2 . Thus, a model with lower values of AICc and BIC is preferred by the data. According to the difference between a given model and the reference one, denoted as ΔAICc , one has the following: if $\Delta\text{AICc} < 4$, both models are supported by the data equally, i.e they are statistically equivalent. If $4 < \Delta\text{AICc} < 10$, the data still support the given model but less than the preferred one. If $\Delta\text{AICc} > 10$, it indicates that the data does not support the given model. Similarly, the difference between a candidate model and the reference model, denoted as ΔBIC , is interpreted in this way: if $\Delta\text{BIC} < 2$, there is no evidence against the candidate model, if $2 < \Delta\text{BIC} < 6$, there is modest evidence against the candidate model, if $6 < \Delta\text{BIC} < 10$, there is strong evidence against the candidate model, and $\Delta\text{BIC} > 10$ gives the strongest evidence against it. Hence, we have performed the above comparison, taking ΛCDM scenario as the reference model, and we display the results in the last two columns of Table 1.

A first observation is that the Kaniadakis parameter β is constrained around 0 as expected, namely around the value in which Kaniadakis entropy recovers the standard Bekenstein-Hawking one. A second observation is that the scenario at hand gives a slightly smaller value for $\Omega_m^{(0)}$ comparing to ΛCDM cosmology, however it estimates a higher value for the present Hubble constant h , closer to its direct measurements through long-period Cepheids. In particular, it is consistent within 1σ with the value reported by [100] and it exhibits a deviation of 0.2σ from the one obtained by Planck [94]. This implies that the scenario of Kaniadakis-holographic dark energy can offer an alleviation to the H_0 tension by reducing the tension in 0.2σ .

Concerning the comparison with ΛCDM scenario, for the combined dataset analysis we find that ΔAICc implies that ΛCDM is only slightly favored over Kaniadakis-holographic dark energy. However, since BIC imposes a stronger penalty to the number of degrees of freedom than AICc , and since Kaniadakis-holographic dark energy has one free parameter more than the concordance model, we find that ΔBIC gives a strong evidence against it.

Finally, based on the combined (CC+SNIa+BAO) analysis, in Fig. 2 we present the reconstruction of the Hubble parameter $H(z)$, the deceleration parameter $q(z)$ (equation (2.26)), and the cosmographic jerk parameter $j(z)$ (equation (2.27)), in the redshift range $0 < z < 2$. For comparison, we also depict the corresponding curves for ΛCDM scenario. Concerning the current values, our analysis leads to $H_0 = 72.23^{+0.98}_{-1.03} \text{ km/s/Mpc}$, $q_0 = -0.551^{+0.068}_{-0.078}$, $j_0 = 0.986^{+0.465}_{-0.300}$, where the uncertainties correspond to 1σ CL. Additionally, using the joint analysis we find the redshift for the deceleration-acceleration transition as $z_T = 0.652^{+0.132}_{-0.108}$, and the Universe age as $t_U = 13.346^{+0.384}_{-0.323} \text{ Gyrs}$. Notice that these values are in agreement

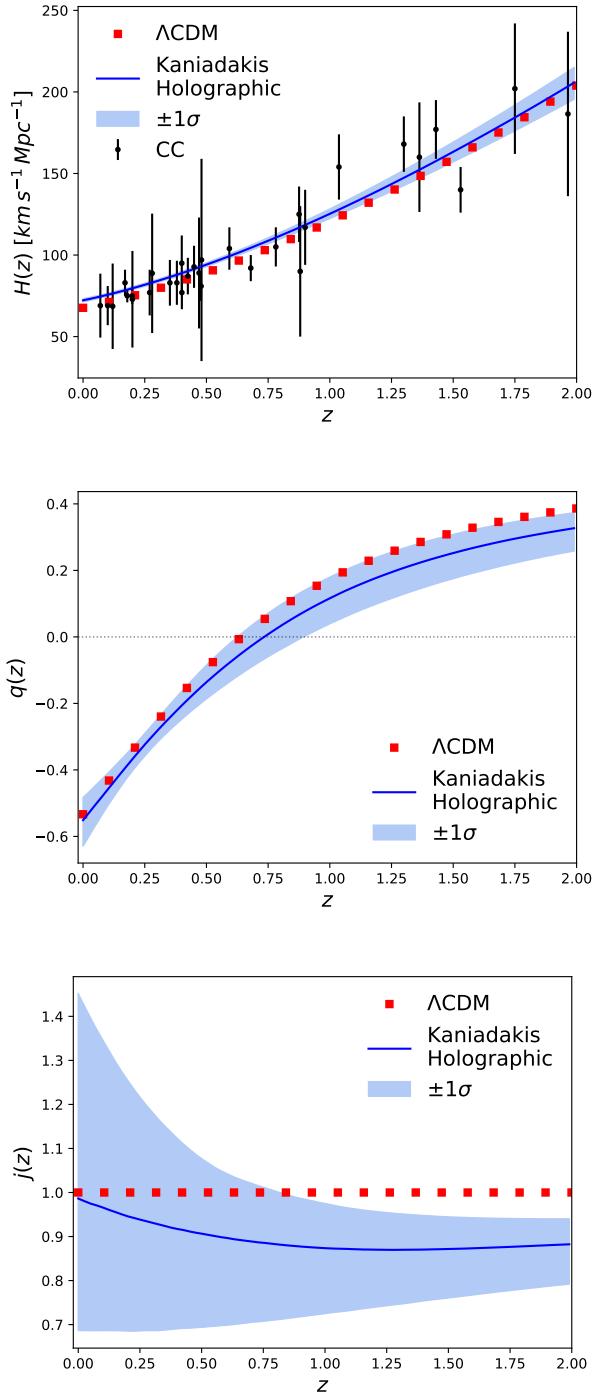


Figure 2. Reconstruction of the Hubble function ($H(z)$, upper panel), the deceleration parameter ($q(z)$, middle panel), and the jerk parameter ($j(z)$, bottom panel) for the Kaniadakis-holographic dark energy using the combined (CC+SNIA+BAO) analysis in the redshift range $0 < z < 2$. The shaded regions represent the 68% confidence level, and the square points depict the results of the Λ CDM scenario with $h = 0.6766$ and $\Omega_m^{(0)} = 0.3111$ [94].

within 1σ with those reported in [101] for Λ CDM paradigm.

4 Dynamical system and stability analysis

In this section we apply the powerful method of phase-space and stability analysis, which allows us to obtain a qualitative description of the local and global dynamics of cosmological scenarios, independently of the initial conditions and the specific evolution of the universe. The extraction of asymptotic solutions give theoretical values that can be compared with the observed ones, such as the dark-energy and total equation-of-state parameters, the deceleration parameter, the density parameters of the different sectors, etc., and also allows the classification of the cosmological solutions [102].

In order to perform the stability analysis of a given cosmological scenario, one transforms it to its autonomous form $\mathbf{X}' = \mathbf{f}(\mathbf{X})$ [15, 102–109], where \mathbf{X} is the column vector containing the auxiliary variables and primes denote derivative with respect to a conveniently chosen time variable. Then, one extracts the critical points \mathbf{X}_c by imposing the condition $\mathbf{X}' = \mathbf{0}$ and, to determine their stability properties, one expands around them with \mathbf{U} the column vector of the perturbations of the variables. Therefore, for each critical point the perturbation equations are expanded to first order as $\mathbf{U}' = \mathbf{Q} \cdot \mathbf{U}$, with the matrix \mathbf{Q} containing the coefficients of the perturbation equations. Finally, the eigenvalues of \mathbf{Q} determine the type and stability of the critical point under consideration.

4.1 Local dynamical system formulation

In this subsection we study the stability of system (2.18)–(2.19) with \mathcal{X} defined in (2.20), in the phase space

$$\{(E, \Omega_{DE}) \in \mathbb{R}^2 : 3E^4\Omega_{DE}^2 - 4\beta^2c^2 \geq 0\}. \quad (4.1)$$

For generality, we keep the matter equation-of-state parameter w_m in the calculations, and it can be set to zero in the final result if needed.

The equilibrium points dominated by dark energy (namely possessing $\Omega_{DE} = 1$) with finite H are:

- $L_1 : (E, \Omega_{DE}) = \left(\frac{\sqrt{2\beta c}}{\sqrt[4]{3}}, 1\right)$. This point always satisfies $-12c^2\beta^2 + 9E^4\Omega_{DE}^2 = 0$. The eigenvalues are $\{-3(w_m + 1), \infty \operatorname{sgn}((\sqrt{2} - 2c))\}$. It is a stable point for $c > \frac{\sqrt{2}}{2}$ and $w_m > -1$, and a saddle for $c < \frac{\sqrt{2}}{2}$ and $w_m > -1$.
- $L_2 : (E, \Omega_{DE}) = \left(\frac{\sqrt{\beta}}{\sqrt[4]{3(1-c^2)}}, 1\right)$. This point satisfies the reality condition if $\frac{3\beta^2(1-2c^2)^2}{1-c^2} \geq 0$, namely $\beta = 0, c^2 > 1$ or $\beta > 0, c^2 < 1$. For $c^2 \leq \frac{1}{2}$ the eigenvalues are $\lambda_1, \lambda_2 = \left\{ \frac{(4c^4-4c^2-1)|c|+(-8c^4+6c^2+1)\sqrt{(1-c^2)}}{|c-2c^3|}, 2\left(\sqrt{\frac{1}{c^2}-1}-1\right)(2c^2-1)-3(w_m+1) \right\}$. This is a saddle point, as it can be verified numerically in Fig. 3. Moreover, for $\frac{1}{2} < c^2 < 1$, the eigenvalues are $\{2-2c^2, -3(w_m+1)\}$, and thus for $w_m > -1$ it is also a saddle point.

Since $\Omega_{DE}^2 \geq \frac{4\beta^2c^2}{3E^4} \geq 0$, we deduce that the only possibility to have matter domination, namely $\Omega_{DE} = 0$, is when $E \rightarrow \infty$, due to the reality condition $c^2\beta^2 \geq 0$. It is convenient to

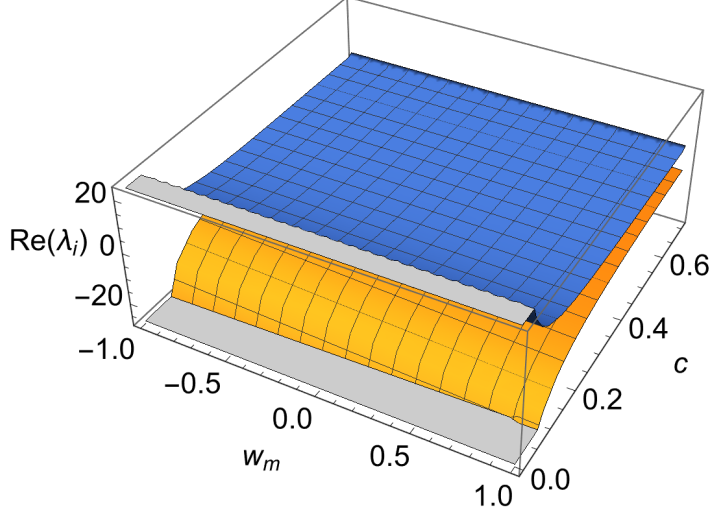


Figure 3. The eigenvalues corresponding to the point L_2 , for $w_m \in [-1, 1]$, $c \in [0, \sqrt{2}/2]$.

define the dimensionless compact variable $T = (1 + E)^{-1}$ such that $T \rightarrow 0$ as $E \rightarrow \infty$ and $T \rightarrow 1$ as $E \rightarrow 0$. Then, we obtain

$$T' = \frac{3}{2}(T-1)T(w_m+1)(\Omega_{DE}-1) - \frac{T^3 \sqrt{\frac{(T-1)^4 \Omega_{DE}^2}{T^4} - \frac{4\beta^2 c^2}{3}}}{T-1} - \frac{\beta T^5 \sqrt{\frac{2(T-1)^4 \Omega_{DE}^2}{T^4} - \frac{8\beta^2 c^2}{3}}}{(T-1)^2 \sqrt{3(T-1)^2 \Omega_{DE} - \sqrt{9(T-1)^4 \Omega_{DE}^2 - 12\beta^2 c^2 T^4}}}, \quad (4.2)$$

$$\Omega'_{DE} = (\Omega_{DE}-1) \left[-3(w_m+1)\Omega_{DE} + \frac{2T^2 \sqrt{\frac{(T-1)^4 \Omega_{DE}^2}{T^4} - \frac{4\beta^2 c^2}{3}}}{(T-1)^2} + \frac{2\beta T^2 \sqrt{2(T-1)^4 \Omega_{DE}^2 - \frac{8}{3}\beta^2 c^2 T^4}}{(T-1)^3 \sqrt{3(T-1)^2 \Omega_{DE} - \sqrt{9(T-1)^4 \Omega_{DE}^2 - 12\beta^2 c^2 T^4}}} \right], \quad (4.3)$$

defined on the physical region

$$9(T-1)^4 \Omega_{DE}^2 - 12\beta^2 c^2 T^4 \geq 0. \quad (4.4)$$

In summary:

- The late-time attractor is the dark-energy dominated solution $L_3 : (T, \Omega_{DE}) = (0, 1)$, for which the eigenvalues are $\left\{ \frac{c-1}{c}, -\frac{3cw_m+c+2}{c} \right\}$, thus it is a stable point for $-1 < w_m < 1$ and $0 < c < 1$.
- The past attractor is the matter dominated solution $L_4 : (T, \Omega_{DE}) = (0, 0)$, for which the eigenvalues are $\left\{ 3(w_m+1), \frac{3(w_m+1)}{2} \right\}$, and since they are always positive for $-1 < w_m < 1$ it is an unstable point.

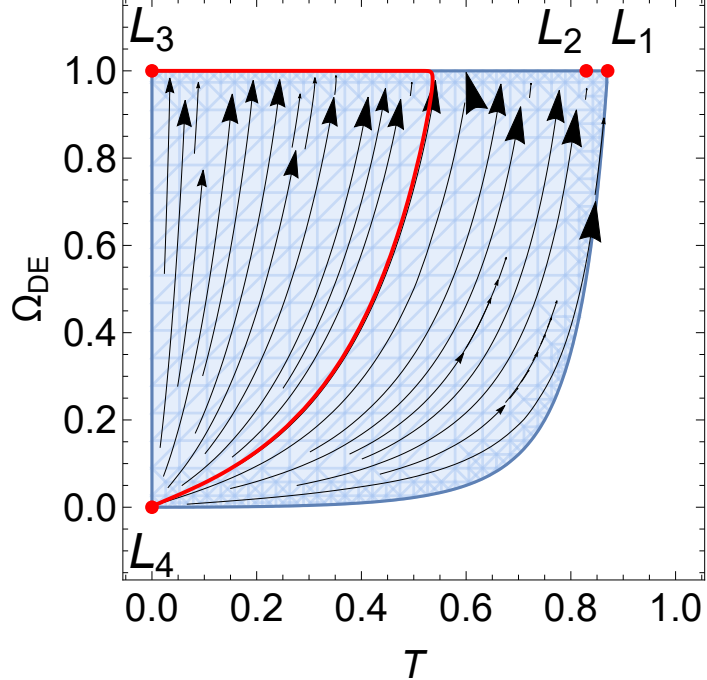


Figure 4. Phase-space plot of the dynamical system (4.2)-(4.3), for the best fit values $\beta = 0.02$ and $c = 0.962$ of Kaniadakis-holographic dark energy, and for dust matter ($w_m = 0$). The red curve represents the solution for the initial data $\Omega_{DE}|_{z=0} = 0.752$, corresponding to the mean value from the joint analysis CC+SNIa+BAO, and for $T|_{z=0} = 0.5$. The dashed blue region is the physical region $9(T - 1)^4 \Omega_{DE}^2 - 12\beta^2 c^2 T^4 \geq 0$, where the equations are real-valued.

We remark here that $E = E_c$ finite corresponds to the de Sitter solution with $H = E_c H_0$, and $a(t) \propto e^{E_c H_0 t}$. That is, point L_1 satisfies $a(t) \propto e^{\frac{\sqrt{2\beta c}}{4\sqrt{3}} H_0 t}$ and it is a late-time attractor providing the accelerated regime. Additionally, point L_2 satisfies $a(t) \propto e^{\frac{\sqrt{\beta}}{4\sqrt{3}(1-c^2)} H_0 t}$, and since it is a saddle it can provide a transient accelerated phase that can be related to inflation.

In order to present the results in a more transparent way, in Fig. 4 we show a phase-space plot of the system (4.2)-(4.3) for the best fit values $\beta = 0.02$ and $c = 0.962$ and for dust matter ($w_m = 0$). The red curve represents the solution for the initial data $\Omega_{DE}|_{z=0} = 0.752$, corresponding to the mean value from the joint analysis CC+SNIa+BAO, and for $T|_{z=0} = 0.5$. The dashed blue region is the physical region $9(T - 1)^4 \Omega_{DE}^2 - 12\beta^2 c^2 T^4 \geq 0$, where the equations are real-valued. From this figure it is confirmed that the late-time attractor is the dark-energy dominated solution $\Omega_{DE} = 1$ with $T = 0$. The past attractor is the matter-dominated solution $\Omega_{DE} = 0$ with $T = 0$. At the finit region, point L_2 is a saddle point, while L_1 is the stable one.

4.2 Global dynamical systems formulation

In the previous subsection we performed the local analysis of the scenario. However, due to the presence of rational functions that are not analytic in the whole domain, it becomes necessary to investigate the full global dynamics. We start by defining the dimensionless

variables θ, T as

$$T = \frac{H_0}{H + H_0} = \frac{1}{1 + E}, \quad \theta = \arcsin \left(\sqrt{1 - \frac{\rho_{DE}}{3M_p^2 H^2}} \right), \quad (4.5)$$

such that

$$\sin^2 \theta = \frac{\rho_m}{3M_p^2 H^2}, \quad \cos^2 \theta = \frac{\rho_{DE}}{3M_p^2 H^2}. \quad (4.6)$$

For an expanding universe ($H > 0$), we have that $T \in [0, 1]$, while θ is a periodic coordinate and, thus, we can set $\theta \in [-\pi, \pi]$. Therefore, we obtain a global phase-space formulation.

4.2.1 Standard holographic dark energy ($\beta = 0$)

In order to present the features of Kaniadakis-holographic dark energy in comparison with standard-holographic dark energy, we first analyze the latter case for completeness, namely we consider the system (2.29a)-(2.29b) for $\beta = 0$. In this case, we obtain

$$T' = \frac{(T - 1)T \{ \cos^2(\theta)[(3w_m + 1)c + 2\cos(\theta)] - 3c(w_m + 1) \}}{2c}, \quad (4.7)$$

$$\theta' = -\frac{[(3w_m + 1)c + 2\cos(\theta)] \sin(2\theta)}{4c}. \quad (4.8)$$

The critical points of the above system, alongside their associated eigenvalues, are presented in Table 2. Note that θ is unique modulo 2π , and focus on $\cos \theta \geq 0$. In the following list $\arctan[x, y]$ gives the arc tangent of y/x , taking into account on which quadrant the point (x, y) is in. When $x^2 + y^2 = 1$, $\arctan[x, y]$ gives the number θ such that $x = \cos \theta$ and $y = \sin \theta$.

Label	(T, θ)	Eigenvalues
P_1	$(0, 2\pi c_1)$	$\left\{ \frac{c-1}{c}, -\frac{3w_m c + c + 2}{2c} \right\}$
P_2	$(0, \frac{1}{2}\pi(4c_1 - 1))$	$\left\{ \frac{3(w_m + 1)}{2}, \frac{1}{2}(3w_m + 1) \right\}$
P_3	$(0, \frac{1}{2}\pi(4c_1 + 1))$	$\left\{ \frac{3(w_m + 1)}{2}, \frac{1}{2}(3w_m + 1) \right\}$
P_4^\pm	$(0, 2\pi c_1 \pm \pi)$	$\left\{ 1 + \frac{1}{c}, -\frac{3w_m}{2} + \frac{1}{c} - \frac{1}{2} \right\}$
P_5	$(0, \arctan[-x, -\sqrt{1 - x^2}] + 2\pi c_1)$	$\left\{ \frac{3(w_m + 1)}{2}, \frac{1}{8}(3w_m + 1)(c^2(1 + 3w_m)^2 - 4) \right\}$
P_6	$(0, \arctan[-x, \sqrt{1 - x^2}] + 2\pi c_1)$	$\left\{ \frac{3(w_m + 1)}{2}, \frac{1}{8}(3w_m + 1)(c^2(1 + 3w_m)^2 - 4) \right\}$
P_7	$(1, 2\pi c_1)$	$\left\{ \frac{1}{c} - 1, -\frac{3w_m c + c + 2}{2c} \right\}$
P_8	$(1, \frac{1}{2}\pi(4c_1 - 1))$	$\left\{ -\frac{3}{2}(w_m + 1), \frac{1}{2}(3w_m + 1) \right\}$
P_9	$(1, \frac{1}{2}\pi(4c_1 + 1))$	$\left\{ -\frac{3}{2}(w_m + 1), \frac{1}{2}(3w_m + 1) \right\}$
P_{10}^\pm	$(1, 2\pi c_1 \pm \pi)$	$\left\{ -\frac{c+1}{c}, -\frac{3w_m}{2} + \frac{1}{c} - \frac{1}{2} \right\}$
P_{11}	$(1, \arctan[-x, -\sqrt{1 - x^2}] + 2\pi c_1)$	$\left\{ -\frac{3}{2}(w_m + 1), \frac{1}{8}(3w_m + 1)(c^2(1 + 3w_m)^2 - 4) \right\}$
P_{12}	$(1, \arctan[-x, \sqrt{1 - x^2}] + 2\pi c_1)$	$\left\{ -\frac{3}{2}(w_m + 1), \frac{1}{8}(3w_m + 1)(c^2(1 + 3w_m)^2 - 4) \right\}$

Table 2. The critical points and their associated eigenvalues of the system (4.7)-(4.8) for $\beta = 0$ in (2.29a)-(2.29b), namely for the case of standard holographic dark energy. We use the notation $x = \frac{1}{2}c(3w_m + 1)$, while $c_1 \in \mathbb{Z}$.

In summary, in the case $\beta = 0$, the critical points can be completely characterized. In particular:

- Point P_1 always exists. It corresponds to a dark-energy dominated solution, i.e. $\Omega_{DE} = 1$ with $T = 0$. It is a stable point for $-1 < w_m < 1$, $0 < c < 1$.
- Points P_2 and P_3 exist always. They are two representations of the matter-dominated solution $\Omega_{DE} = 0$ with $T = 0$. They are past attractors, i.e. unstable points, for $-\frac{1}{3} < w_m \leq 1$, while they are saddle for $-1 < w_m < -\frac{1}{3}$.
- Points P_4^\pm exist always. They correspond to the dark-energy dominated solution with $\Omega_{DE} = 1$ with $T = 0$. They are unstable points for $0 < c < \frac{1}{2}$, $-1 \leq w_m \leq 1$, or $c \geq \frac{1}{2}$, $-1 \leq w_m < \frac{2-c}{3c}$, while they are saddle for $c > \frac{1}{2}$, $\frac{2-c}{3c} < w_m \leq 1$.
- Points P_5 and P_6 exist for $-1 \leq \frac{1}{2}c(3w_m + 1) \leq 1$. They are sources for $0 \leq c \leq 1$, $-1 < w_m < -\frac{1}{3}$ or $c > 1$, $-\frac{c+2}{3c} < w_m < -\frac{1}{3}$. For $0 \leq c < \frac{1}{2}$, $-\frac{1}{3} < w_m \leq 1$, or $c \geq \frac{1}{2}$, $-\frac{1}{3} < w_m < \frac{2-c}{3c}$, they are saddle.
- Point P_7 exists always. It corresponds to a dark-energy dominated solution $\Omega_{DE} = 1$ with $T = 1$. It is a stable point for $c > 1$, $-\frac{c+2}{3c} < w_m \leq 1$.
- Points P_8 and P_9 exist always. They are two representations of the matter-dominated solution $\Omega_{DE} = 0$ with $T = 1$. They are stable points for $-1 < w_m < -\frac{1}{3}$, while they are saddle points for $-\frac{1}{3} < w_m \leq 1$.
- Points P_{10}^\pm are two representations of the matter-dominated solution $\Omega_{DE} = 0$ with $T = 1$. They are stable points for $c > \frac{1}{2}$, $\frac{2-c}{3c} < w_m \leq 1$, while they are saddle for $0 < c < \frac{1}{2}$, $-1 \leq w_m \leq 1$, or $c \geq \frac{1}{2}$, $-1 \leq w_m < \frac{2-c}{3c}$.
- Points P_{11} and P_{12} exist for $-1 \leq \frac{1}{2}c(3w_m + 1) \leq 1$. They are saddle for $0 \leq c \leq 1$, $-1 < w_m < -\frac{1}{3}$ or $c > 1$, $-\frac{c+2}{3c} < w_m < -\frac{1}{3}$, while for $0 \leq c < \frac{1}{2}$, $-\frac{1}{3} < w_m \leq 1$, or $c \geq \frac{1}{2}$, $-\frac{1}{3} < w_m < \frac{2-c}{3c}$, they are stable.

In order to give a better picture of the system behavior, Fig. 5 display a phase-space plot of the system (4.7)-(4.8) for $\beta = 0$ in (2.29a)-(2.29b), and dust matter. The red curve corresponds to the universe evolution according to parameter mean values from the joint analysis. From this figure we deduce that the late-time attractor is the dark-energy dominated solution with $\Omega_{DE} = 1$ and $T = 0$ (point P_1), while the past attractor is the matter-dominated solution with $\Omega_{DE} = 0$ and $T = 0$ (point P_3). For other initial conditions there are other late-time attractors, such as points P_{11} and P_{12} which are stable for the best-fit parameters since they satisfy $c \geq \frac{1}{2}$, $-\frac{1}{3} < w_m < \frac{2-c}{3c}$. These points are scaling solutions since they have $\Omega_{DE} = x^2$ and $\Omega_{DM} = 1 - x^2$, with $x = \frac{c}{2}(3w_m + 1) = \frac{c}{2}$ for $w_m = 0$. Additionally, points P_2 , P_3 , which are matter-dominated solutions, and points P_4^\pm , which are dark-energy dominated solutions, are also past attractors.

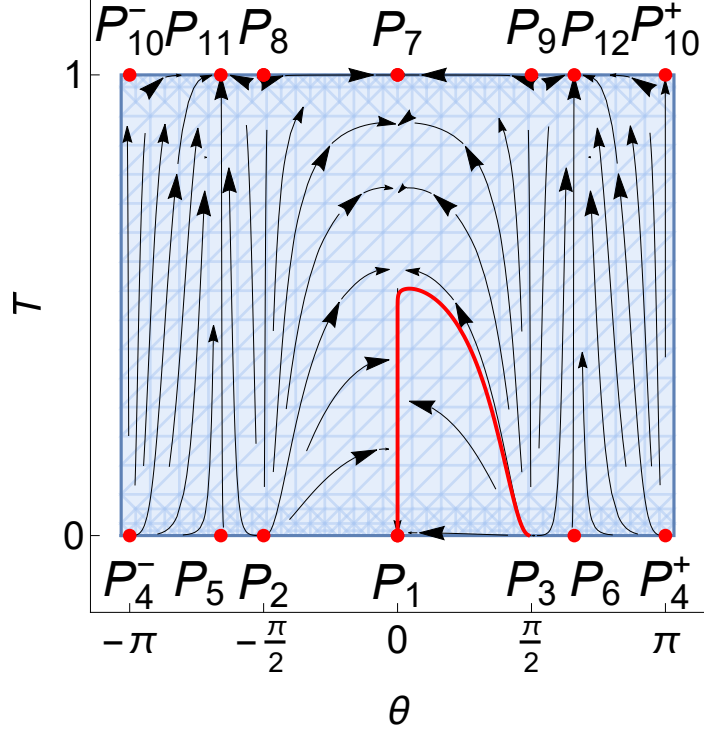


Figure 5. Phase-space plot of the dynamical system (4.7)-(4.8) for $\beta = 0$ in (2.29a)-(2.29b), namely for standard holographic dark energy, for the value $c = 0.962$, and for dust matter $w_m = 0$. The red curve represents the solution for the initial data $\Omega_{DE}|_{z=0} = 0.752$ (i.e., $\theta(0) = \arccos\left(\frac{1}{5}\sqrt{\frac{94}{5}}\right) \approx 0.521$), corresponding to the mean value obtained with the joint analysis $CC+SNIa+BAO$, and for $T|_{z=0} = 0.5$. The dashed blue region is the physical region where the equations are real-valued.

4.2.2 Kaniadakis holographic dark energy ($\beta \neq 0$)

Let us now investigate the full extended model of Kaniadakis holographic dark energy, namely the general case where $\beta \neq 0$. The full system (2.18)-(2.19) becomes

$$T' = \frac{3}{2}(1-T)T(w_m + 1)\sin^2(\theta) + \frac{T^3\sqrt{\frac{(1-T)^4\cos^4(\theta)}{T^4} - \frac{4\beta^2c^2}{3}}}{1-T} - \frac{\beta T^5\sqrt{\frac{18(1-T)^4\cos^4(\theta)}{T^4} - 24\beta^2c^2}}{3(T-1)^2\sqrt{3(T-1)^2\cos^2(\theta) - \sqrt{9(1-T)^4\cos^4(\theta) - 12\beta^2c^2T^4}}}, \quad (4.9)$$

$$\theta' = -\frac{3}{4}(w_m + 1)\sin(2\theta) + \frac{T^2\tan(\theta)\sqrt{\frac{(1-T)^4\cos^4(\theta)}{T^4} - \frac{4\beta^2c^2}{3}}}{(T-1)^2} - \frac{\sqrt{\frac{2}{3}}T^2\tan(\theta)\sqrt{-\beta^2(4\beta^2c^2T^4 - 3(1-T)^4\cos^4(\theta))}}{(1-T)^3\sqrt{3(T-1)^2\cos^2(\theta) - \sqrt{9(1-T)^4\cos^4(\theta) - 12\beta^2c^2T^4}}}. \quad (4.10)$$

Moreover, the physical region of the phase space is

$$3(1-T)^4\cos^4(\theta) - 4\beta^2c^2T^4 \geq 0. \quad (4.11)$$

We proceed by studying the critical points of the system (4.9)-(4.10) in the physical region (4.11) and their stability. We mention that for $\beta \neq 0$ the invariant set $T = 1$ is not physical. Near the invariant set $T = 0$ the system (4.9)-(4.10) becomes

$$T' = \left[-\frac{\cos^3(\theta)}{c} + \cos^2(\theta) + \frac{3}{2}(w_m + 1) \sin^2(\theta) \right] T + O(T^2), \quad (4.12)$$

$$\theta' = -\frac{[(3w_m + 1)c + 2\cos(\theta)]\sin(2\theta)}{4c} + O(T^2). \quad (4.13)$$

In Table 3 we summarize the critical points P_1 to P_6 , alongside their associated eigenvalues. Furthermore, the stability conditions are the same as discussed in subsection 4.2.1. In summary, in the invariant set $T = 0$, the critical points are:

- Point P_1 exists always. It corresponds to a dark-energy dominated solution, i.e. $\Omega_{DE} = 1$ with $T = 0$. It is a stable point for $-1 < w_m < 1$, $0 < c < 1$.
- Points P_2 and P_3 exist always. They are two representations of the matter-dominated solution $\Omega_{DE} = 0$ with $T = 0$. They are past attractors, i.e. unstable points, for $-\frac{1}{3} < w_m \leq 1$, while they are saddle for $-1 < w_m < -\frac{1}{3}$.
- Points P_4^\pm exist always. They correspond to the dark-energy dominated solution with $\Omega_{DE} = 1$ with $T = 0$. They are unstable points for $0 < c < \frac{1}{2}$, $-1 \leq w_m \leq 1$, or $c \geq \frac{1}{2}$, $-1 \leq w_m < \frac{2-c}{3c}$, while they are saddle for $c > \frac{1}{2}$, $\frac{2-c}{3c} < w_m \leq 1$.
- Points P_5 and P_6 exist for $-1 \leq \frac{1}{2}c(3w_m + 1) \leq 1$. They are unstable for $0 \leq c \leq 1$, $-1 < w_m < -\frac{1}{3}$ or $c > 1$, $-\frac{c+2}{3c} < w_m < -\frac{1}{3}$, while for $0 \leq c < \frac{1}{2}$, $-\frac{1}{3} < w_m \leq 1$, or $c \geq \frac{1}{2}$, $-\frac{1}{3} < w_m < \frac{2-c}{3c}$, they are saddle.

Moreover, the system admits, at most, twelve additional equilibrium points (θ, T) , with $\theta \in \{\theta_1, \theta_2, \theta_3\}$ satisfying $\cos^2(\theta) = 1$, and $T \in \{T_1, T_2, T_3, T_4\}$ satisfying $\frac{(T-1)^4}{T^4} - \frac{4\beta^2 c^2}{3} = 0$. Explicitly, we have that

$$\theta_1 = 2\pi c_1, \quad \theta_{2,3} = \pm\pi + 2\pi c_1$$

if $c_1 \in \mathbb{Z}$, and

$$T_{1,2} = -\frac{2\sqrt{3}\beta c}{|4\beta^2 c^2 - 3|} + \frac{3}{3 - 4\beta^2 c^2} \mp \sqrt{2} \sqrt{\frac{\beta c (16\sqrt{3}\beta^4 c^4 + 12\beta c|4\beta^2 c^2 - 3| - 9\sqrt{3})}{|4\beta^2 c^2 - 3|^3}},$$

$$T_{3,4} = \frac{2\sqrt{3}\beta c}{|4\beta^2 c^2 - 3|} + \frac{3}{3 - 4\beta^2 c^2} \mp \sqrt{2} \sqrt{\frac{\beta c (-16\sqrt{3}\beta^4 c^4 + 12\beta c|4\beta^2 c^2 - 3| + 9\sqrt{3})}{|4\beta^2 c^2 - 3|^3}}}.$$

Notice that the physical values are the real values of T_i satisfying $0 \leq T_i \leq 1$, $i = 1, 2, 3, 4$. One eigenvalue is always $-\frac{3}{2}(1 + w_m)$, while the other one is infinite. The stability conditions are found numerically and, moreover, for $\beta = 0$ we find $T_i = 0$. Hence, we re-obtain points P_7 and P_{10}^\pm in Table 2. Indeed, for $\beta = 0$ all the results of section 4.2.1 are recovered.

The solutions of physical interest are those with $T = 0$. Point P_1 , which corresponds to a dark-energy dominated solution $\Omega_{DE} = 1$ with $T = 0$, is stable for $-1 < w_m < 1$, $0 < c < 1$. Points P_2 and P_3 , which are two representations of the matter-dominated solution $\Omega_{DE} = 0$ with $T = 0$, are past attractors for $-\frac{1}{3} < w_m \leq 1$ or saddle for $-1 < w_m < -\frac{1}{3}$. Points P_4^\pm , which correspond to a dark-energy dominated solution are unstable for $0 < c < \frac{1}{2}$, $-1 \leq$

Label	(T, θ)	Eigenvalues
P_1	$(0, 2\pi c_1)$	$\left\{ \frac{c-1}{c}, -\frac{3w_m c + c + 2}{2c} \right\}$
P_2	$(0, \frac{1}{2}\pi (4c_1 - 1))$	$\left\{ \frac{3(w_m + 1)}{2}, \frac{1}{2}(3w_m + 1) \right\}$
P_3	$(0, \frac{1}{2}\pi (4c_1 + 1))$	$\left\{ \frac{3(w_m + 1)}{2}, \frac{1}{2}(3w_m + 1) \right\}$
P_4^\pm	$(0, 2\pi c_1 \pm \pi)$	$\left\{ 1 + \frac{1}{c}, -\frac{3w_m}{2} + \frac{1}{c} - \frac{1}{2} \right\}$
P_5	$(0, \arctan[-x, -\sqrt{1-x^2}] + 2\pi c_1)$	$\left\{ \frac{3(w_m + 1)}{2}, \frac{1}{8}(3w_m + 1)(c^2(1 + 3w_m)^2 - 4) \right\}$
P_6	$(0, \arctan[-x, \sqrt{1-x^2}] + 2\pi c_1)$	$\left\{ \frac{3(w_m + 1)}{2}, \frac{1}{8}(3w_m + 1)(c^2(1 + 3w_m)^2 - 4) \right\}$

Table 3. The critical points and their associated eigenvalues of the system (4.9)-(4.10) in the invariant set $T = 0$. We use the notation $x = \frac{1}{2}c(3w_m + 1)$, $c_1 \in \mathbb{Z}$.

$w_m \leq 1$, or $c \geq \frac{1}{2}$, $-1 \leq w_m < \frac{2-c}{3c}$, while they are saddle points for $c > \frac{1}{2}$, $\frac{2-c}{3c} < w_m \leq 1$. Finally, points P_5 and P_6 exist for $-1 \leq \frac{1}{2}c(3w_m + 1) \leq 1$. They are sources for $0 \leq c \leq 1$, $-1 < w_m < -\frac{1}{3}$ or $c > 1$, $-\frac{c+2}{3c} < w_m < -\frac{1}{3}$, while for $0 \leq c < \frac{1}{2}$, $-\frac{1}{3} < w_m \leq 1$, or $c \geq \frac{1}{2}$, $-\frac{1}{3} < w_m < \frac{2-c}{3c}$, they are saddle. Finally, note that the region where $T \rightarrow 1$ is contained in the complex-valued domain. This forbids solutions with $H = 0$, which appear in the standard-holographic dark energy scenario of (4.7)-(4.8).

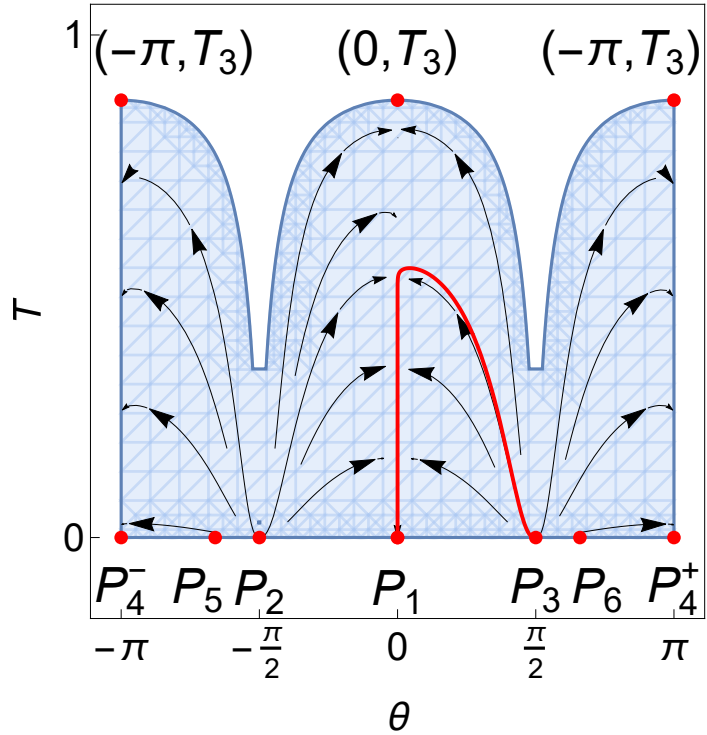


Figure 6. Phase-space plot of the dynamical system (4.9)-(4.10) for the best fit values $\beta = 0.02$ and $c = 0.962$, and for dust matter ($w_m = 0$). The red curve represents the solution for the initial data $\Omega_{DE}|_{z=0} = 0.752$ (i.e., $\theta(0) = \arccos\left(\frac{1}{5}\sqrt{\frac{94}{5}}\right) \approx 0.521$), corresponding to the mean value from the joint analysis CC+SNIA+BAO, and for $T|_{z=0} = 0.5$. The dashed-blue region is the physical region where the equations are real-valued.

In Fig. 6 we show a phase-space plot of the system (4.9)-(4.10) for the best-fit values $\beta = 0.02$ and $c = 0.962$ and for dust matter ($w_m = 0$). In this case the only real value is $T_3 = 0.87$. At points $(-\pi, T_3)$, $(0, T_3)$, and (π, T_3) , the eigenvalues are $\{9.78 \times 10^6, -\frac{3}{2}\}$ and one eigenvalue is positive infinity at the exact value of T_3 , therefore they are saddles. For comparison, we have added the red curve, corresponding to the solution for the initial data $\Omega_{DE}|_{z=0} = 0.752$ (i.e., $\theta(0) = \arccos\left(\frac{1}{5}\sqrt{\frac{94}{5}}\right) \approx 0.521$), which is the mean value from the joint analysis CC+SNIa+BAO, and for $T|_{z=0} = 0.5$. From this figure it is confirmed that the late-time attractor is the dark-energy dominated solution while the past attractor is the matter-dominated solution.

5 Summary and discussion

We investigated the scenario of Kaniadakis-holographic dark energy scenario by confronting it with observational data. This is an extension of the usual holographic dark-energy model which arises from the use of the generalized Kaniadakis entropy instead of the standard Boltzmann-Gibbs one, which in turn appear from the relativistic extension of standard statistical theory.

We applied the Bayesian approach to extract the likelihood bounds of the Kaniadakis parameter, as well as the other free model parameters. In particular, we performed a Markov Chain Monte Carlo analysis using data from cosmic chronometers, supernovae type Ia, and Baryon Acoustic Oscillations observations. Concerning the Kaniadakis parameter, we found that it is constrained around 0, namely, around the value in which Kaniadakis entropy recovers the standard Bekenstein-Hawking one, as expected. Additionally, for $\Omega_m^{(0)}$ we obtained a slightly smaller value compared to Λ CDM scenario. However, the interesting result is that for the present Hubble constant the combined dataset analysis gave $h = 0.722_{-0.010}^{+0.010}$, which is consistent within 1σ with its direct measurements, and thus Kaniadakis-holographic dark energy offers an alleviation to the H_0 tension.

Furthermore, we reconstructed the evolution of the Hubble, deceleration and jerk parameters in the redshift range $0 < z < 2$. We find that, within one sigma confidence level, the deceleration-acceleration transition redshift is $z_T = 0.65_{-0.11}^{+0.13}$, and the age of the Universe is $t_U = 13.346_{-0.323}^{+0.384}$ Gyrs. Lastly, we applied the usual information criteria in order to compare the statistical significance of the fittings with Λ CDM cosmology. According to AICc the Λ CDM scenario is only slightly favored in comparison to Kaniadakis-holographic dark energy, while BIC finds Λ CDM cosmology is strongly preferred because it has one less parameter than Kaniadakis-holographic dark energy.

Finally, we performed a detailed dynamical-system analysis to extract the local and global features of the evolution in the scenario of Kaniadakis-holographic dark energy. We extracted the critical points as well as their stability properties and found that the past attractor of the Universe is the matter-dominated solution, while the late-time stable solution is the dark-energy-dominated one.

In summary, Kaniadakis-holographic dark energy presents interesting cosmological behavior and is in agreement with observations. The fact that it can alleviate the H_0 tension by providing a H_0 value very close to its direct measurements, may be considered as a significant advantage. These features make it worthy of further investigation.

Acknowledgments

G.L. was funded by Agencia Nacional de Investigación y Desarrollo - ANID for financial support through the program FONDECYT Iniciación grant no. 11180126 and by Vicerrectoría de Investigación y Desarrollo Tecnológico at UCN. J.M. acknowledges the support from ANID project Basal AFB-170002 and ANID REDES 190147. M.A.G.-A. acknowledges support from SNI-México, CONACyT research fellow, ANID REDES (190147) and Instituto Avanzado de Cosmología (IAC). A.H.A. thanks to the PRODEP project, Mexico for resources and financial support and thanks also to the support from Luis Aguilar, Alejandro de León, Carlos Flores, and Jair García of the Laboratorio Nacional de Visualización Científica Avanzada. V.M. acknowledges support from Centro de Astrofísica de Valparaíso and ANID REDES 190147. This work is partially supported by the Ministry of Education and Science of the Republic of Kazakhstan, Grant AP08856912.

References

- [1] A.G. Riess, A.V. Filippenko, P. Challis, A. Clocchiatti, A. Diercks et al., *Observational evidence from supernovae for an accelerating universe and a cosmological constant*, *The Astronomical Journal* **116** (1998) 1009.
- [2] S. Perlmutter, G. Aldering, G. Goldhaber, R.A. Knop, P. Nugent, others et al., *Measurements of ω and λ from 42 high-redshift supernovae*, *The Astrophysical Journal* **517** (1999) 565.
- [3] WMAP collaboration, *First year Wilkinson Microwave Anisotropy Probe (WMAP) observations: Determination of cosmological parameters*, *Astrophys. J. Suppl.* **148** (2003) 175 [[astro-ph/0302209](#)].
- [4] S. Nadathur, W.J. Percival, F. Beutler and H. Winther, *Testing Low-Redshift Cosmic Acceleration with Large-Scale Structure*, *Phys. Rev. Lett.* **124** (2020) 221301 [[2001.11044](#)].
- [5] Y. Zel'dovich, A. Krasinski and Y. Zeldovich, *The Cosmological constant and the theory of elementary particles*, *Sov. Phys. Usp.* **11** (1968) 381.
- [6] S. Weinberg, *The cosmological constant problem*, *Rev. Mod. Phys.* **61** (1989) 1.
- [7] A.G. Riess, S. Casertano, W. Yuan, J.B. Bowers, L. Macri, J.C. Zinn et al., *Cosmic Distances Calibrated to 1% Precision with Gaia EDR3 Parallaxes and Hubble Space Telescope Photometry of 75 Milky Way Cepheids Confirm Tension with Λ CDM*, *Astrophys. J. Lett.* **908** (2021) L6 [[2012.08534](#)].
- [8] PLANCK collaboration, *Planck 2018 results. VI. Cosmological parameters*, [1807.06209](#).
- [9] E. Di Valentino et al., *Snowmass2021 - Letter of interest cosmology intertwined II: The hubble constant tension*, *Astropart. Phys.* **131** (2021) 102605 [[2008.11284](#)].
- [10] DES collaboration, *STRIDES: a 3.9 per cent measurement of the Hubble constant from the strong lens system DES J0408-5354*, *Mon. Not. Roy. Astron. Soc.* **494** (2020) 6072 [[1910.06306](#)].
- [11] S. Birrer and T. Treu, *TDCOSMO. V. Strategies for precise and accurate measurements of the Hubble constant with strong lensing*, *Astronomy & Astrophysics* **649** (2021) A61 [[2008.06157](#)].
- [12] G. Efstathiou, *To H_0 or not to H_0 ?*, *Mon. Not. Roy. Astron. Soc.* **505** (2021) 3866 [[2103.08723](#)].
- [13] W.L. Freedman, *Measurements of the Hubble Constant: Tensions in Perspective*, [2106.15656](#).
- [14] P. Shah, P. Lemos and O. Lahav, *A buyer's guide to the Hubble Constant*, [2109.01161](#).

[15] E.J. Copeland, M. Sami and S. Tsujikawa, *Dynamics of dark energy*, *Int. J. Mod. Phys. D* **15** (2006) 1753 [[hep-th/0603057](#)].

[16] Y.-F. Cai, E.N. Saridakis, M.R. Setare and J.-Q. Xia, *Quintom Cosmology: Theoretical implications and observations*, *Phys. Rept.* **493** (2010) 1 [[0909.2776](#)].

[17] V. Motta, M.A. García-Aspeitia, A. Hernández-Almada, J. Magaña and T. Verdugo, *Taxonomy of dark energy models*, *Universe* **7** (2021) .

[18] S.A. Chaplygin, , *Sci. Mem. Moscow Univ. Math. Phys.* **21** (1904) .

[19] J. Villanueva, *The generalized chaplygin-jacobi gas*, *Journal of Cosmology and Astroparticle Physics* **2015** (2015) 045.

[20] Hernández-Almada, A., Magaña, Juan, García-Aspeitia, Miguel A. and Motta, V., *Cosmological constraints on alternative model to chaplygin fluid revisited*, *Eur. Phys. J. C* **79** (2019) 12.

[21] M. Cruz, N. Cruz and S. Lepe, *Accelerated and decelerated expansion in a causal dissipative cosmology*, *Phys. Rev. D* **96** (2017) 124020.

[22] M. Cruz, N. Cruz and S. Lepe, *Accelerated and decelerated expansion in a causal dissipative cosmology*, *Phys. Rev. D* **96** (2017) 124020.

[23] N. Cruz, A. Hernández-Almada and O. Cornejo-Pérez, *Constraining a causal dissipative cosmological model*, *Phys. Rev. D* **100** (2019) 083524.

[24] A. Hernández-Almada, *Cosmological test on viscous bulk models using Hubble parameter measurements and type Ia supernovae data*, *The European Physical Journal C* **79** (2019) 751.

[25] A. Hernández-Almada, M.A. García-Aspeitia, J. Magana and V. Motta, *Stability analysis and constraints on interacting viscous cosmology*, *Phys. Rev. D* **101** (2020) 063516 [[2001.08667](#)].

[26] A. Hernández-Almada, M.A. García-Aspeitia, J. Magaña and V. Motta, *Stability analysis and constraints on interacting viscous cosmology*, *Phys. Rev. D* **101** (2020) 063516.

[27] CANTATA collaboration, *Modified Gravity and Cosmology: An Update by the CANTATA Network*, [2105.12582](#).

[28] S. Capozziello and M. De Laurentis, *Extended Theories of Gravity*, *Phys. Rept.* **509** (2011) 167 [[1108.6266](#)].

[29] R. Maartens and K. Koyama, *Brane-World Gravity*, *Living Rev. Rel.* **13** (2010) 5 [[1004.3962](#)].

[30] M.A. García-Aspeitia, J. Magaña, A. Hernández-Almada and V. Motta, *Probing dark energy with braneworld cosmology in the light of recent cosmological data*, *Int. J. Mod. Phys. D* **27** (2017) 1850006 [[1609.08220](#)].

[31] M.A. Garcia-Aspeitia, A. Hernandez-Almada, J. Magaña, M.H. Amante, V. Motta and C. Martínez-Robles, *Brane with variable tension as a possible solution to the problem of the late cosmic acceleration*, *Phys. Rev. D* **97** (2018) 101301 [[1804.05085](#)].

[32] X. Li and A. Shafieloo, *A Simple Phenomenological Emergent Dark Energy Model can Resolve the Hubble Tension*, *The Astrophysical Journal Letters* **883** (2019) L3 [[1906.08275](#)].

[33] S. Pan, W. Yang, E. Di Valentino, A. Shafieloo and S. Chakraborty, *Reconciling H_0 tension in a six parameter space?*, *arXiv e-prints* (2019) arXiv:1907.12551 [[1907.12551](#)].

[34] X. Li and A. Shafieloo, *Generalised Emergent Dark Energy Model: Confronting Λ and PEDE*, *arXiv e-prints* (2020) arXiv:2001.05103 [[2001.05103](#)].

[35] A. Hernández-Almada, G. Leon, J. Magaña, M.A. García-Aspeitia and V. Motta, *Generalized Emergent Dark Energy: observational Hubble data constraints and stability analysis*, *Mon. Not. Roy. Astron. Soc.* **497** (2020) 1590 [[2002.12881](#)].

[36] M.A. García-Aspeitia, C. Martínez-Robles, A. Hernández-Almada, J. Magaña and V. Motta, *Cosmic acceleration in unimodular gravity*, *Phys. Rev.* **D99** (2019) 123525 [[1903.06344](#)].

[37] M.A. García-Aspeitia, A. Hernández-Almada, J. Magaña and V. Motta, *The Universe acceleration from the Unimodular gravity view point: Background and linear perturbations*, *Phys. Dark Univ.* **32** (2021) 100840 [[1912.07500](#)].

[38] D. Glavan and C. Lin, *Einstein-Gauss-Bonnet Gravity in Four-Dimensional Spacetime*, *Phys. Rev. Lett.* **124** (2020) 081301 [[1905.03601](#)].

[39] M.A. García-Aspeitia and A. Hernández-Almada, *Einstein-Gauss-Bonnet gravity: Is it compatible with modern cosmology?*, *Phys. Dark Univ.* **32** (2021) 100799 [[2007.06730](#)].

[40] E.N. Saridakis and S. Basilakos, *The generalized second law of thermodynamics with Barrow entropy*, [2005.08258](#).

[41] G. Leon, J. Magaña, A. Hernández-Almada, M.A. García-Aspeitia, T. Verdugo and V. Motta, *Barrow Entropy Cosmology: an observational approach with a hint of stability analysis*, [2108.10998](#).

[42] Y.-F. Cai, S. Capozziello, M. De Laurentis and E.N. Saridakis, *$f(T)$ teleparallel gravity and cosmology*, *Rept. Prog. Phys.* **79** (2016) 106901 [[1511.07586](#)].

[43] G. 't Hooft, *Dimensional Reduction in Quantum Gravity*, *arXiv e-prints* (1993) gr [[gr-qc/9310026](#)].

[44] L. Susskind, *The world as a hologram*, *Journal of Mathematical Physics* **36** (1995) 6377 [[hep-th/9409089](#)].

[45] M. Li, *A Model of holographic dark energy*, *Phys. Lett. B* **603** (2004) 1 [[hep-th/0403127](#)].

[46] S. Wang, Y. Wang and M. Li, *Holographic Dark Energy*, *Phys. Rept.* **696** (2017) 1 [[1612.00345](#)].

[47] R. Horvat, *Holography and variable cosmological constant*, *Phys. Rev. D* **70** (2004) 087301 [[astro-ph/0404204](#)].

[48] D. Pavon and W. Zimdahl, *Holographic dark energy and cosmic coincidence*, *Phys. Lett. B* **628** (2005) 206 [[gr-qc/0505020](#)].

[49] B. Wang, Y.-g. Gong and E. Abdalla, *Transition of the dark energy equation of state in an interacting holographic dark energy model*, *Phys. Lett. B* **624** (2005) 141 [[hep-th/0506069](#)].

[50] S. Nojiri and S.D. Odintsov, *Unifying phantom inflation with late-time acceleration: Scalar phantom-non-phantom transition model and generalized holographic dark energy*, *Gen. Rel. Grav.* **38** (2006) 1285 [[hep-th/0506212](#)].

[51] H. Kim, H.W. Lee and Y.S. Myung, *Equation of state for an interacting holographic dark energy model*, *Phys. Lett. B* **632** (2006) 605 [[gr-qc/0509040](#)].

[52] M.R. Setare and E.N. Saridakis, *Non-minimally coupled canonical, phantom and quintom models of holographic dark energy*, *Phys. Lett. B* **671** (2009) 331 [[0810.0645](#)].

[53] M.R. Setare and E.N. Saridakis, *Correspondence between Holographic and Gauss-Bonnet dark energy models*, *Phys. Lett. B* **670** (2008) 1 [[0810.3296](#)].

[54] X. Zhang and F.-Q. Wu, *Constraints on holographic dark energy from Type Ia supernova observations*, *Phys. Rev. D* **72** (2005) 043524 [[astro-ph/0506310](#)].

[55] M. Li, X.-D. Li, S. Wang and X. Zhang, *Holographic dark energy models: A comparison from the latest observational data*, *JCAP* **06** (2009) 036 [[0904.0928](#)].

[56] C. Feng, B. Wang, Y. Gong and R.-K. Su, *Testing the viability of the interacting holographic dark energy model by using combined observational constraints*, *JCAP* **09** (2007) 005 [[0706.4033](#)].

[57] X. Zhang, *Holographic Ricci dark energy: Current observational constraints, quintom feature, and the reconstruction of scalar-field dark energy*, *Phys. Rev. D* **79** (2009) 103509 [[0901.2262](#)].

[58] J. Lu, E.N. Saridakis, M.R. Setare and L. Xu, *Observational constraints on holographic dark energy with varying gravitational constant*, *JCAP* **03** (2010) 031 [[0912.0923](#)].

[59] S.M.R. Micheletti, *Observational constraints on holographic tachyonic dark energy in interaction with dark matter*, *JCAP* **05** (2010) 009 [[0912.3992](#)].

[60] Y.-g. Gong, *Extended holographic dark energy*, *Phys. Rev. D* **70** (2004) 064029 [[hep-th/0404030](#)].

[61] E.N. Saridakis, *Restoring holographic dark energy in brane cosmology*, *Phys. Lett. B* **660** (2008) 138 [[0712.2228](#)].

[62] R.-G. Cai, *A Dark Energy Model Characterized by the Age of the Universe*, *Phys. Lett. B* **657** (2007) 228 [[0707.4049](#)].

[63] M.R. Setare and E.C. Vagenas, *Thermodynamical Interpretation of the Interacting Holographic Dark Energy Model in a non-flat Universe*, *Phys. Lett. B* **666** (2008) 111 [[0801.4478](#)].

[64] E.N. Saridakis, *Holographic Dark Energy in Braneworld Models with Moving Branes and the $w=-1$ Crossing*, *JCAP* **04** (2008) 020 [[0712.2672](#)].

[65] M. Suwa and T. Nihei, *Observational constraints on the interacting Ricci dark energy model*, *Phys. Rev. D* **81** (2010) 023519 [[0911.4810](#)].

[66] M. Bouhmadi-Lopez, A. Errahmani and T. Ouali, *The cosmology of an holographic induced gravity model with curvature effects*, *Phys. Rev. D* **84** (2011) 083508 [[1104.1181](#)].

[67] M. Khurshudyan, J. Sadeghi, R. Myrzakulov, A. Pasqua and H. Farahani, *Interacting quintessence dark energy models in Lyra manifold*, *Adv. High Energy Phys.* **2014** (2014) 878092 [[1404.2141](#)].

[68] E.N. Saridakis, *Ricci-Gauss-Bonnet holographic dark energy*, *Phys. Rev. D* **97** (2018) 064035 [[1707.09331](#)].

[69] S. Nojiri and S.D. Odintsov, *Covariant Generalized Holographic Dark Energy and Accelerating Universe*, *Eur. Phys. J. C* **77** (2017) 528 [[1703.06372](#)].

[70] E.N. Saridakis, K. Bamba, R. Myrzakulov and F.K. Anagnostopoulos, *Holographic dark energy through Tsallis entropy*, *JCAP* **12** (2018) 012 [[1806.01301](#)].

[71] C. Kritpetch, C. Muhammad and B. Gumjudpai, *Holographic dark energy with non-minimal derivative coupling to gravity effects*, *Phys. Dark Univ.* **30** (2020) 100712 [[2004.06214](#)].

[72] E.N. Saridakis, *Barrow holographic dark energy*, *Phys. Rev. D* **102** (2020) 123525 [[2005.04115](#)].

[73] M.P. Dabrowski and V. Salzano, *Geometrical observational bounds on a fractal horizon holographic dark energy*, *Phys. Rev. D* **102** (2020) 064047 [[2009.08306](#)].

[74] W.J.C. da Silva and R. Silva, *Cosmological Perturbations in the Tsallis Holographic Dark Energy Scenarios*, *Eur. Phys. J. Plus* **136** (2021) 543 [[2011.09520](#)].

[75] A.A. Mamon, A. Paliathanasis and S. Saha, *Dynamics of an Interacting Barrow Holographic Dark Energy Model and its Thermodynamic Implications*, *Eur. Phys. J. Plus* **136** (2021) 134 [[2007.16020](#)].

[76] S. Bhattacharjee, *Growth Rate and Configurational Entropy in Tsallis Holographic Dark Energy*, *Eur. Phys. J. C* **81** (2021) 217 [[2011.13135](#)].

[77] Q. Huang, H. Huang, B. Xu, F. Tu and J. Chen, *Dynamical analysis and statefinder of Barrow holographic dark energy*, *Eur. Phys. J. C* **81** (2021) 686.

[78] C. Lin, *An effective field theory of holographic dark energy*, [2101.08092](#).

[79] E.O. Colgáin and M.M. Sheikh-Jabbari, *A critique of holographic dark energy*, *Class. Quant. Grav.* **38** (2021) 177001 [[2102.09816](#)].

[80] S. Nojiri, S.D. Odintsov and T. Paul, *Different Faces of Generalized Holographic Dark Energy*, *Symmetry* **13** (2021) 928 [[2105.08438](#)].

[81] S.H. Shekh, *Models of holographic dark energy in $f(Q)$ gravity*, *Phys. Dark Univ.* **33** (2021) 100850.

[82] N. Drepanou, A. Lymeris, E.N. Saridakis and K. Yesmakhanova, *Kaniadakis holographic dark energy*, [2109.09181](#).

[83] G. Kaniadakis, *Statistical mechanics in the context of special relativity*, *Phys. Rev. E* **66** (2002) 056125 [[cond-mat/0210467](#)].

[84] G. Kaniadakis, *Statistical mechanics in the context of special relativity. II.*, *Phys. Rev. E* **72** (2005) 036108 [[cond-mat/0507311](#)].

[85] E.M.C. Abreu, J. Ananias Neto, E.M. Barboza and R.C. Nunes, *Jeans instability criterion from the viewpoint of Kaniadakis' statistics*, *EPL* **114** (2016) 55001 [[1603.00296](#)].

[86] E.M.C. Abreu, J.A. Neto, A.C.R. Mendes and A. Bonilla, *Tsallis and Kaniadakis statistics from a point of view of the holographic equipartition law*, *EPL* **121** (2018) 45002 [[1711.06513](#)].

[87] E.M.C. Abreu and J. Ananias Neto, *Black holes thermodynamics from a dual Kaniadakis entropy*, *EPL* **133** (2021) 49001.

[88] H. Moradpour, A.H. Ziae and M. Kord Zangeneh, *Generalized entropies and corresponding holographic dark energy models*, *Eur. Phys. J. C* **80** (2020) 732 [[2005.06271](#)].

[89] A. Lymeris, S. Basilakos and E.N. Saridakis, *Modified cosmology through Kaniadakis horizon entropy*, [2108.12366](#).

[90] M. Moresco, L. Pozzetti, A. Cimatti, R. Jimenez, C. Maraston, L. Verde et al., *A 6% measurement of the Hubble parameter at $z \sim 0.45$: direct evidence of the epoch of cosmic re-acceleration*, *JCAP* **1605** (2016) 014 [[1601.01701](#)].

[91] J. Magaña, M.H. Amante, M.A. García-Aspeitia and V. Motta, *The cardassian expansion revisited: constraints from updated hubble parameter measurements and type ia supernova data*, *Monthly Notices of the Royal Astronomical Society* **476** (2018) 1036 [[1706.09848](#)].

[92] D.M. Scolnic et al., *The Complete Light-curve Sample of Spectroscopically Confirmed SNe Ia from Pan-STARRS1 and Cosmological Constraints from the Combined Pantheon Sample*, *Astrophys. J.* **859** (2018) 101 [[1710.00845](#)].

[93] R.C. Nunes, S.K. Yadav, J.F. Jesus and A. Bernui, *Cosmological parameter analyses using transversal bao data*, *Monthly Notices of the Royal Astronomical Society* **497** (2020) 2133–2141.

[94] N. Aghanim, Y. Akrami, M. Ashdown, J. Aumont, C. Baccigalupi, M. Ballardini et al., *Planck 2018 results*, *Astronomy & Astrophysics* **641** (2020) A6.

[95] D. Foreman-Mackey, D.W. Hogg, D. Lang and J. Goodman, *emcee: The MCMC Hammer*, *pasp* **125** (2013) 306 [[1202.3665](#)].

[96] H. Akaike, *A new look at the statistical model identification*, *IEEE Transactions on Automatic Control* **19** (1974) 716.

[97] N. Sugiura, *Further analysts of the data by akaike's information criterion and the finite corrections*, *Communications in Statistics - Theory and Methods* **7** (1978) 13.

[98] C.M. Hurvich and C.L. Tsai, *Regression and time series model selection in small samples*, *Biometrika* **76** (1989) 297.

[99] G. Schwarz, *Estimating the dimension of a model*, *Ann. Statist.* **6** (1978) 461.

- [100] A.G. Riess, S. Casertano, W. Yuan, L.M. Macri and D. Scolnic, *Large magellanic cloud cepheid standards provide a 1% foundation for the determination of the hubble constant and stronger evidence for physics beyond Λ cdm*, *The Astrophysical Journal* **876** (2019) 85.
- [101] L. Herrera-Zamorano, A. Hernández-Almada and M.A. García-Aspeitia, *Constraints and cosmography of Λ CDM in presence of viscosity*, *The European Physical Journal C* **80** (2020) .
- [102] J. Wainwright and G.F.R. Ellis, *Dynamical Systems in Cosmology*, Cambridge University Press (1997).
- [103] P.G. Ferreira and M. Joyce, *Structure formation with a selftuning scalar field*, *Phys. Rev. Lett.* **79** (1997) 4740 [[astro-ph/9707286](#)].
- [104] E.J. Copeland, A.R. Liddle and D. Wands, *Exponential potentials and cosmological scaling solutions*, *Phys. Rev. D* **57** (1998) 4686 [[gr-qc/9711068](#)].
- [105] L. Perko, *Differential Equations and Dynamical Systems, Third Edition*, Springer (2000).
- [106] A.A. Coley, *Dynamical systems and cosmology*, vol. 291, Kluwer, Dordrecht, Netherlands (2003), [10.1007/978-94-017-0327-7](#).
- [107] X.-m. Chen, Y.-g. Gong and E.N. Saridakis, *Phase-space analysis of interacting phantom cosmology*, *JCAP* **0904** (2009) 001 [[0812.1117](#)].
- [108] S. Cotsakis and G. Kittou, *Flat limits of curved interacting cosmic fluids*, *Phys. Rev. D* **88** (2013) 083514 [[1307.0377](#)].
- [109] R. Giambò and J. Miritzis, *Energy exchange for homogeneous and isotropic universes with a scalar field coupled to matter*, *Class. Quant. Grav.* **27** (2010) 095003 [[0908.3452](#)].